# First observation of energetic neutral atoms in the Venus environment

A. Galli [a,*], P. Wurz [a], P. Bochsler [a], S. Barabash [b], A. Grigoriev [b], Y. Futaana [b],
M. Holmström [b], H. Gunell [b], H. Andersson [b], R. Lundin [b], M. Yamauchi [b], K. Brinkfeldt [b],
M. Fraenz [c], N. Krupp [c], J. Woch [c], W. Baumjohann [d], H. Lammer [d], T. L. Zhang [d],
K. Asamura [e], A. J. Coates [f], D. R. Linder [f], D. O. Kataria [f], C. C. Curtis [g], K. C. Hsieh [g],
B. R. Sandel [g], J. A. Sauvaud [h], A. Fedorov [h], C. Mazelle [h], J. J. Thocaven [h], M. Grande [i],
E. Kallio [j], T. Sales [j], W. Schmidt [j], P. Riihela [j], H. Koskinen [k,j], J. Kozyra [ℓ], J. Luhmann [m],
S. McKenna-Lawlor [n], S. Orsini [o], R. Cerulli-Irelli [o], A. Mura [o], A. Milillo [o], M. Maggi [o],
E. Roelof [p], P. Brandt [p], C. T. Russell [q], K. Szego [r], D. Winningham [s], R. Frahm [s],
J. Scherrer [s], J. R. Sharber [s]

[a] *Physikalisches Institut, University of Bern, Bern, Switzerland*
[b] *Swedish Institute of Space Physics, Kiruna, Sweden*
[c] *Max-Planck Institut für Sonnensystemforschung, Katlenburg-Lindau, Germany*
[d] *Space Research Institute, Austrian Academy of Sciences, Graz, Austria*
[e] *Institute of Space and Astronautical Science, Sagamichara, Japan*
[f] *Mullard Space Science Laboratory, University College London, Surrey, UK*
[g] *University of Arizona, Tucson, USA*
[h] *Centre d'Etude Spatiale des Rayonnements, Toulouse, France*
[i] *Rutherford Appleton Laboratory, Chilton, UK*
[j] *Finnish Meteorological Institute, Helsinki, Finland*
[k] *University of Helsinki, Department of Physical Sciences, Helsinki, Finland*
[ℓ] *Space Physics Research Laboratory, University of Michigan, Ann Arbor, USA*
[m] *Space Science Laboratory, University of California at Berkeley, Berkeley, USA*
[n] *Space Technology Ireland, National University of Ireland, Maynooth, Ireland*
[o] *Istituto di Fisica dello Spazio Interplanetario, Rome, Italy*
[p] *Applied Physics Laboratory, Johns Hopkins University, Laurel, USA*
[q] *Institute of Geophysics and Planetary Physics, University of California, Los Angeles, USA*
[r] *KFKI Research Institute for Particle and Nuclear Physics, Budapest, Hungary*
[s] *Southwest Research Institute, San Antonio, USA*

## Abstract

The ASPERA-4 instrument on board the Venus Express spacecraft offers for the first time the possibility to directly measure the emission of energetic neutral atoms (ENAs) in the vicinity of Venus. When the spacecraft is inside the Venus shadow a distinct signal of hydrogen ENAs usually is detected. It is observed as a narrow tailward stream, coming from the dayside exosphere around the Sun direction. The intensity of the signal reaches several $10^5$ cm$^{-2}$ sr$^{-1}$ s$^{-1}$, which is consistent with present theories of the plasma and neutral particle distributions around Venus.

*Key words:* Venus exosphere, ENAs, Solar wind-planetary atmosphere interaction

## 1. Introduction

In the past, several spacecraft exploring Venus have locally measured the atmosphere and ionosphere, but before ESA's Venus Express (VEX) none has imaged the emission of ENAs in the Venus environment. Theoretical models (Fok et al., 2004; Gunell et al., 2005) have predicted that the flux of hydrogen and oxygen ENAs around Venus should be high enough to be detectable by present instrumentation at any time during the solar cycle.

An ENA is produced in a charge-exchange collision of a fast ion (either a solar wind ion or an accelerated planetary ion) with an exospheric neutral atom. An ENA signal, $j_{ENA}$, observed at some distance from the planet, can be interpreted as a line-of-sight integral over the ion intensity $j_{ion}$ through the planetary exosphere:

$$j_{ENA} = \int j_{ion}(\sigma_{H,ion} n_H + \sigma_{O,ion} n_O) \; dl_{LOS}$$

where $\sigma$ is the charge-exchange cross section. At Venus, the two most important neutral species for charge-exchange reactions are atomic hydrogen and oxygen (Fok et al., 2004). The ENA intensity is sensitive to the neutral density profiles, $n_H$ and $n_O$, and to the plasma distributions around Venus. ENA measurements allow global imaging of the interaction of the solar wind with the Venusian ionosphere and atmosphere. They constrain the models of plasma populations (Biernat et al., 1999; Tanaka & Murawski, 1997), of exospheric densities (Keating et al., 1985), and of the atmospheric loss of H and O (Lammer et al., 2006). They also can be compared to the recent ENA measurements at Mars (Galli et al., 2007).

## 2. Instrumentation

The ASPERA-4 instrument on VEX is a copy of the ASPERA-3 instrument, which is still operational in Mars orbit. It consists of an ion mass analyser, an electron spectrometer and two neutral particle sensors (Barabash et al., 2007). In this letter we report on the first data collected with the neutral particle detector (NPD). NPD is sensitive to neutral H and O atoms in the energy range from 0.2 to 10 keV, and uses the time-of-flight (TOF) technique for energy analysis. We interpret the ENAs

* Corresponding author. Tel.: +41 31 631 85 34; fax: +41 31 631 44 05.
   *Email address:* galli@space.unibe.ch (A. Galli).

reported here as hydrogen ENAs, because we have not detected yet any distinct TOF signal of O-ENAs between 0.2 and 1 keV (corresponding to TOF bins 100 to 256 in Fig. 2) at a detection threshold of a few $10^4$ $cm^{-2}$ $sr^{-1}$ $s^{-1}$. $O^+$ ions faster than 1 keV do exist in the tail behind Venus (Luhmann et al., 2006); such an O-ENA would produce a TOF signal that we are now ascribing to an H-ENA. However, neutral exosphere (Keating et al., 1985) and plasma models (Kallio et al., 2006) indicate that O-ENA signals at energies above 1 keV are unlikely to reach intensities as high as we have measured.

For data evaluation the registered TOF spectra (in counts $s^{-1}$) are converted to differential energy spectra ($cm^{-2}$ $sr^{-1}$ $s^{-1}$ $keV^{-1}$) with the method developed for ASPERA-3/NPD (Galli et al., 2006). At present, only preliminary calibration parameters are available for spectrum reconstruction. The resulting error is expected to be $\leq 20\%$ of the presented values for the ENA intensity and the roll-over.

## 3. Observations

The measurements obtained in the Venus shadow show the most unambiguous and most intense ENA signals seen with VEX/NPD up to now. Here, we restrict ourselves to the first two eclipse seasons (May 2006 and August 2006). During these periods NPD was switched on while in Venus shadow on 27 different orbits. For data evaluation we have concentrated on those 13 orbits for which the observation time was longer than 10 minutes, and the NPD FOV covered the hemisphere around Venus. From the 27 original orbits we have excluded all observations for which the direction of the ENA signal coincides with the position of the solar panel. This data set is summarised in Table 1.

Typically, the instrument was switched on after pericenter passage and collected data for 15 minutes while the spacecraft was moving away from Venus at a solar zenith angle of 130° to 160°. The altitude increased from 700 to 4000 km until the spacecraft left the Venus shadow. As an example, the orbit on May 24, 2006, is shown in Fig. 1. While inside the shadow the ASPERA-4 platform was rotating rapidly between 0° and 180° around the instrument axis. This allowed us to cover a big portion of the full sky at the price of a poor spatial resolution.

In 10 out of 13 orbits through eclipse when the NPD FOV is directed towards the sunward hemisphere a distinct hydrogen ENA signal is detected
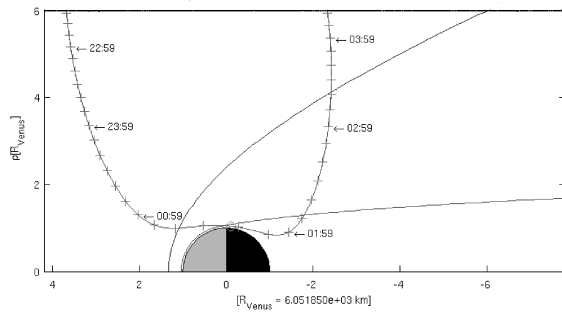
Figure 1. VEX orbit on May 24, 2006, in the Venus Solar Orbital frame (cylindrical coordinates). NPD collected data from 01:44 UT until 01:56 inside the eclipse while the spacecraft was moving away from the planet. The outer line around Venus denotes the bow shock, the inner plasma boundary, which VEX crossed at 02:10, is the ionosheath boundary.

with a median intensity of $1.8 \times 10^5$ cm$^{-2}$ sr$^{-1}$ s$^{-1}$. It is observed when the NPD FOV covers the region around the Venus limb within 30° of the Sun direction. The roll-over of the energy spectra varies among different ENA measurements between 0.4 and 1.6 keV, but the shapes of the energy spectra have to be regarded with caution because the integration times are only a few minutes. A typical example is the orbit on May 24, 2006, when we measure $j_{\mathrm{ENA}} = (1.5 \pm 0.4) \times 10^5$ cm$^{-2}$ sr$^{-1}$ s$^{-1}$ (Fig. 2).

According to the models by Fok et al. (2004) and Gunell et al. (2005) the principal production region of solar wind ENAs is the dayside exosphere above the subsolar point, inside the bow shock. Towards the Sun direction a second favoured region is predicted due to solar wind protons that charge-exchange before reaching the bow shock. For eclipse observations with solar zenith angles close to 180° the two production regions add to one single ENA spot around the Venus limb, the highest intensities occurring close to the Sun direction. The NPD observations confirm the theoretical picture: In 10 out of the 10 cases where an unambiguous ENA signal is detected the ENA intensity reaches its maximum around the Venus limb close to the Sun direction. This is illustrated by the contour plot in Fig. 3.

The statistics of all investigated orbits are shown in Table 1. On 13 among the 27 different orbits through the eclipse the observation conditions were favourable to investigate the Venus limb. The other 14 measurement were too short or the Venus limb was outside the FOV or the solar panel of the spacecraft obstructed the FOV. In 10 out of the 13 orbits an unambiguous ENA signal is detected, in 3 orbits the maximum ENA intensity around the Venus



VEX/NPD: Field–of–view
2006 May 24 01:50:13
Altitude = 1847 km
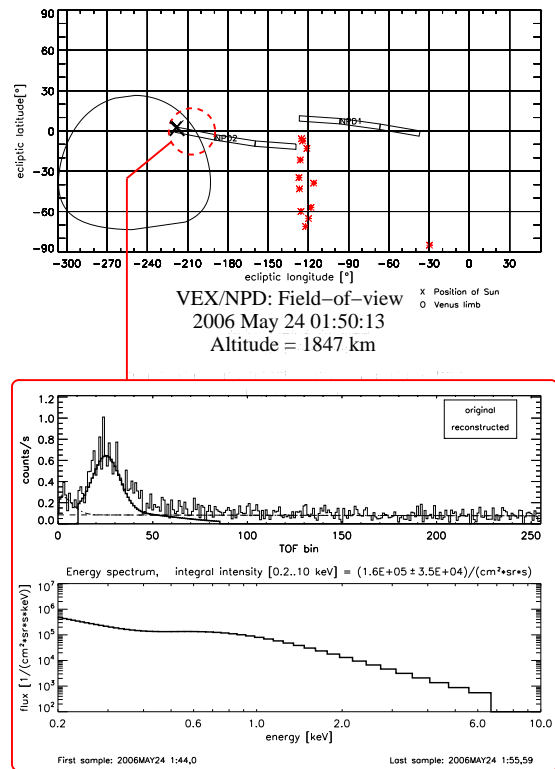


Figure 2. Typical example of ENAs measured in Venus eclipse. The upper plot shows the pointing direction of the six channels of NPD (rectangles) in ecliptic longitude and latitude, the position of the solar panel is sketched with red stars. The middle panel shows the TOF spectrum (each of the 256 bins represents 8 ns) of the ENAs entering from the Sun direction, the lower panel shows the reconstructed differential energy spectrum (roll-over at 0.8 keV). In the TOF spectrum, the UV background (dashed line) and the spurious signal in the first TOF bins (dash-dotted line) have been subtracted from the original measurement (thin line) to get the reconstructed values (thick line).

limb does not cross the detection threshold (a few $10^4$ cm$^{-2}$ sr$^{-1}$ s$^{-1}$). From the space more than 60° away from Venus we detect in 0 out of 18 orbits an ENA signal above this detection limit.

## 4. Conclusions

We see ENAs on the nightside of Venus. In 10 out of 13 orbits where we observe the Venus limb we detect a distinct ENA signal, with intensities $(1 \text{ to } 3) \times 10^5$ cm$^{-2}$ sr$^{-1}$ s$^{-1}$ between 0.2 and 10 keV. This ENA signal is restricted to the region around the Venus limb within 30° of the Sun direction. We conclude that we predominantly observe solar wind

| | |
|---|---|
| Total number of orbits | 27 |
| Number of suitable orbits | 18 |
| ENA signals detected at $> 60°$ away from Venus limb | 0 |
| Orbits suitable for Venus limb observations | 13 |
| Orbits during which ENAs are detected around Venus | 10 |
| Median intensity of all ENA signals | $1.8 \times 10^5 \mathrm{cm}^{-2}$ $\mathrm{sr}^{-1}$ $\mathrm{s}^{-1}$ |
| Most intense ENA signal | $(3 \pm 1) \times 10^5 \mathrm{cm}^{-2}$ $\mathrm{sr}^{-1}$ $\mathrm{s}^{-1}$ |

Table 1

Data set of eclipse measurements.
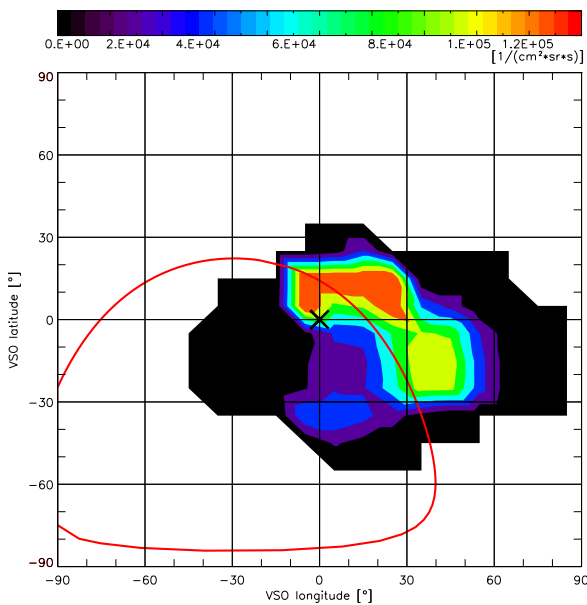


Figure 3. Contour plot of ENA intensities ($\mathrm{cm}^{-2}$ $\mathrm{sr}^{-1}$ $\mathrm{s}^{-1}$), averaged over all 9 orbits where the Venus limb (red silhouette) was covered and the spacecraft altitude was below 0.5 Venus radii. The coloured area corresponds to those directions that have been observed on more than one orbit. Because of the fast spacecraft motion, the scanner rotation and the required 10 to 20 minutes of integration time we cannot resolve yet the size of the ENA production region more accurately than $30°$. It is restricted to the region around the Venus limb close to the Sun direction (cross).

protons that have been neutralised in the dayside exosphere: The ENA production region, on 13 different orbits, always coincides with the Sun direction, whereas ENAs of planetary pick up ions would be aligned with the electric field of the solar wind, fluctuating randomly around the Venus limb from orbit to orbit as the IMF configuration changes. The integral intensities also agree with the model predic-

tions for solar wind ENAs (Gunell et al., 2005).

The intensities and the spatial distribution of H-ENAs around Venus are similar to those measured with ASPERA-3/NPD on the nightside of Mars (Galli et al., 2007), with the difference that Venus is a narrower ENA source. Once the NPD FOV is $60°$ away from the direction of maximum intensity we do not detect any ENA signal (at a detection limit of a few $10^4$ $\mathrm{cm}^{-2}$ $\mathrm{sr}^{-1}$ $\mathrm{s}^{-1}$). This is expected because at Venus the exospheric densities fall off much more rapidly with altitude than at Mars.

## References

Barabash, S., et al., 2007. The Analyzer of Space Plasma and Energetic Atoms (ASPERA-4) for the Venus Express Mission. P&SS, in press.

Biernat, H.K., Erkaev, N.V., Farrugia, C.J., 1999. Aspects of MHD flow about Venus. JGR 104, 12617.

Fok, M.-C., Moore, T.E., Collier, M.R., 2004. Neutral atom imaging of solar wind interaction with the Earth and Venus. JGR 109, A01206.

Galli, A., et al., 2006. Direct measurements of energetic neutral hydrogen in the interplanetary medium. ApJ 644, 1317.

Galli, A., Wurz, P., Barabash, S., Grigoriev, A., Gunell, H., Lundin, R., Holmström, M., Fedorov, A., 2007. Energetic hydrogen and oxygen atoms observed on the nightside of Mars. SSR, in press.

Gunell, H., Holmström, M., Biernat, H.K., Erkaev, N.V., 2005. Planetary ENA imaging: Venus and a comparison with Mars. P&SS 53, 433.

Kallio, E., Jarvinen, R., Janhunen, P., 2006. Venus-solar wind interaction: Asymmetries and the escape of $O^+$ ions. P&SS 54, 1472.

Keating, G.M., et al., 1985. Models of Venus neutral upper atmosphere: structure and composition. AdvSR Vol. 5 Is. 11, 117.

Lammer, H., et al., 2006. Loss of hydrogen and oxygen from the upper atmosphere of Venus. P&SS 54, 1445.

Luhmann, J.G., Ledvina, S.A., Lyon, J.G., Russell, C.T., 2006. Venus $O^+$ pickup ions: Collected PVO results and expectations for Venus Express, P&SS 54, 1457.

Tanaka, T., Murawski, K., 1997. Three-dimensional MHD simulation of the solar wind interaction with the ionosphere of Venus: Results of two-component reacting plasma simulation. JGR 102, 19805.